HHS Public Access

Author manuscript

Neuroimage. Author manuscript; available in PMC 2017 January 15.

Published in final edited form as:

Neuroimage. 2016 January 15; 125: 233–243. doi:10.1016/j.neuroimage.2015.10.014.

Lateralization of Cervical Spinal Cord Activity during an Isometric Upper Extremity Motor Task with Functional Magnetic Resonance Imaging

Kenneth A. Weber II[a], **Yufen Chen**[a], **Xue Wang**[a], **Thorsten Kahnt**[b], and **Todd B. Parrish**[a]

[a]Department of Radiology, Northwestern University, 737 North Michigan Avenue, Suite 1600, Chicago, IL 60611, USA

[b]Department of Neurology, Northwestern University, 303 East Chicago Avenue, Ward 13-006, Chicago, IL 60611, USA

Abstract

The purpose of this study was to use an isometric upper extremity motor task to detect activity induced blood oxygen level dependent signal changes in the cervical spinal cord with functional magnetic resonance imaging. Eleven healthy volunteers performed six 5 minute runs of an alternating left- and right-sided isometric wrist flexion task, during which images of the cervical spinal cord were acquired with a reduced field-of-view T2*-weighted gradient-echo echo-planar-imaging sequence. Spatial normalization to a standard spinal cord template was performed, and average group activation maps were generated in a mixed-effects analysis. The task activity significantly exceeded that of the control analyses. The activity was lateralized to the hemicord ipsilateral to the task and reliable across the runs at the group and subject level. Finally, a multi-voxel pattern analysis was able to successfully decode the left and right tasks at the C6 and C7 vertebral levels.

Keywords

Humans; Functional MRI; Spinal Cord; Motor Activity; Upper Extremity; Functional Laterality

1. Introduction

In humans, the execution of skilled voluntary movements results primarily from descending excitatory inputs from the contralateral cortical motor areas through the crossing fibers of the corticospinal tract to the motoneurons in the anterior horn of the spinal cord ipsilateral to the movement (Jenny and Inukai, 1983; Lemon and Griffiths, 2005). Shortly after the introduction of the blood oxygen level dependent contrast (BOLD), studies demonstrating

Corresponding Author. Kenneth A. Weber II, DC, PhD Candidate, Interdepartmental Neuroscience Program, Department of Radiology, Northwestern University, 737 North Michigan Avenue Suite 1600, Chicago, IL 60611, +1 847-997-6299 (Mobile), +1 312-695-1626 (Work), kweber@u.northwestern.edu.

the feasibility of using functional magnetic resonance imaging (fMRI) to non-invasively detect motor-related brain activity were published (Bandettini et al., 1992; Joliot et al., 1999; Kim et al., 1993; Kwong et al., 1992; van Gelderen et al., 1995). The characteristic finding from these studies was the robust lateralization of the activity to the contralateral motor and sensory cortices, which is consistent with our understanding of the brain regions involved in the execution of voluntary skilled movements (Cincotta and Ziemann, 2008).

Following the success of the early brain fMRI studies, several independent groups have attempted to use fMRI to detect motor-related spinal cord activity. The development of spinal cord fMRI, however, has been slower than brain fMRI due to several technical difficulties with the imaging of the spinal cord and the analysis of functional spinal cord images (Fratini et al., 2014; Stroman et al., 2014). Despite these challenges, the field has continued to progress, and spinal cord fMRI has been used to detect motor-related activity during several different motor tasks including repetitive finger flexion and extension (Bouwman et al., 2008; Yoshizawa et al., 1996), repetitive squeezing of a ball (Giulietti et al., 2008; Stroman et al., 2001; Stroman et al., 1999; Stroman and Ryner, 2001), repetitive fist clenching (Backes et al., 2001; Ng et al., 2006), repetitive elbow flexion and extension (Madi et al., 2001), repetitive wrist extension and flexion (Madi et al., 2001), repetitive finger abduction and adduction (Madi et al., 2001), holding weights in a flexed arm position (Madi et al., 2001), repetitive tongue movements to activate the infrahyoid muscles (Komisaruk et al., 2002), pedaling (Kornelsen and Stroman, 2004, 2007), repetitive thumb to finger apposition (Maieron et al., 2007; Ng et al., 2008; Vahdat et al., 2015), and repetitive finger tapping (Govers et al., 2007; Xie et al., 2009).

As in the brain, lateralization of the activity to the ipsilateral motor (anterior horn) and sensory (posterior horn) areas of the spinal cord during the execution of skilled voluntary movements should be expected with spinal cord fMRI. However, the lateralization of spinal cord activity has not been reliably shown in the previous motor studies. In fact, only a few of the spinal cord fMRI motor studies quantitatively assessed the laterality of the activity (Bouwman et al., 2008; Govers et al., 2007; Maieron et al., 2007; Ng et al., 2008; Stroman et al., 1999; Xie et al., 2009; Yoshizawa et al., 1996). Of these studies, only three statistically assessed the degree of laterality across the subjects, and only Maieron et al. 2007 detected significant lateralization of the activity to the ipsilateral hemicord across the subjects (Bouwman et al., 2008; Maieron et al., 2007; Ng et al., 2008).

The shortfall of reported lateralization of the spinal cord activity in the previous studies may be due to the complexity of the motor tasks employed (e.g., repetitive thumb to finger apposition). The motor tasks required the coordinated reciprocal activation and relaxation of multiple muscle groups and likely produced an influx of neural activity from multiple cutaneous, joint, and muscle afferents. Thus, the resulting fMRI signal in the spinal cord was likely a complex summation of multiple motor, interneuronal, and sensory processes, which may have impeded the detection of task-related signal changes and the localization of activity within the spinal cord. In contrast, a less complex isometric motor task may allow for more robust signal detection in the spinal cord as the motoneuron activity and sensory inputs should remain more stable over a block of activation.

The purpose of this study was to use an isometric left- and right-sided wrist flexion task in order to minimize the complexity of the neural signal and robustly detect and localize the fMRI signal in the spinal cord. In order to determine that the signal being detected is physiological in origin and not artifactual, we test whether the activation rate exceeds the false positive rate, examine the anatomical specificity of the activity, and determine the reliability of the signal. Additional advancements with this study include the use of reduced field-of-view imaging and spatial normalization to a standard template (Cohen-Adad et al., 2014; Rieseberg et al., 2002).

2. Material and methods

2.1 Participants

Eleven healthy volunteers (5 male and 6 female; average age ± one standard deviation (SD) 27.7 ± 1.9 years) were studied. Subjects reported no neurological or musculoskeletal diseases or contraindications to MRI. Each subject provided written informed consent, and the entire study protocol was approved by Northwestern University's Institutional Review Board.

2.2 Data acquisition

Imaging was performed with a 3.0 Tesla Siemens (Erlangen, Germany) Prisma magnetic resonance (MR) scanner equipped with a 64-channel head/neck coil (anterior and posterior neck coils were used (24 channels) and head coils 1–4 were turned off). Subjects were placed supine on the scanner bed. A SatPad™ cervical collar was used to increase the magnetic field homogeneity across the cervical spine and to reduce bulk motion during scanning (Maehara et al., 2014). For the functional images, thirty-one transverse slices of the cervical spinal cord were acquired with a T2*-weighted gradient-echo echo-planar-imaging sequence using ZOOMit selective field-of-view imaging (TR = 2500 ms, TE = 30 ms, flip angle = 80°, acquisition matrix = 128 × 128, field-of-view = 128 × 128 mm^2, in-plane resolution = 1 × 1 mm^2, slice thickness = 3 mm, discarded 2 dummy volumes) (Pfeuffer et al., 2002; Rieseberg et al., 2002). The imaged volume spanned from the inferior endplate of the third cervical vertebra to the superior endplate of the first thoracic vertebra. For registration of the functional images to standard space, a high-resolution T2-weighted structural image of the entire cervical spine and upper thoracic spine was acquired using a single slab 3D turbo spin echo sequence with a slab selective, variable excitation pulse (SPACE, TR = 1500 ms, TE_{eff} = 115 ms, echo train length = 78, flip angle = 90°/140°, resolution = 0.4 × 0.4 × 0.8 mm^3) (Lichy et al., 2005; Mugler et al., 2000).

During functional imaging, the subjects performed an alternating left- and right-sided upper extremity isometric motor task. Rigid plastic resting hand splints were used to immobilize the wrist and hand bilaterally. When prompted by visual instructions presented during scanning, the subjects were trained to produce and maintain a constant flexion force at the left or right wrist of about 50% of their maximum force output. The subjects performed six 15 s trials of left wrist flexion and six 15 s trials of right wrist flexion per run. The order of the trials was pseudorandomized, each trial was separated by a varying duration rest period for a total time of 5 min per run, and each subject performed six runs. A 5 min task free

(resting state) run was also collected for control purposes. Throughout imaging, the subjects were instructed to remain still and not produce any other movements. Subject performance was observed by the study personnel throughout each run.

2.3 Motion correction

Image preprocessing and statistical analyses were performed using the Oxford Center for fMRI of the Brain's (FMRIB) Software Library (FSL) (Jenkinson et al., 2012; Smith et al., 2004). Motion correction was performed using FMRIB's Linear Image Registration Tool with spline interpolation and a normalized correlation cost function (Jenkinson et al., 2002). To exclude areas of non-rigid motion outside of the vertebral column, a manually drawn binary mask of the vertebral column was used to weight the reference image. For the first phase of motion correction, the images across the runs were realigned to the first image of the first run with three-dimensional rigid body realignment. To correct for slice independent motion due to the non-rigidity of the cervical spine and physiological motion from swallowing and the respiratory cycle, a second phase of motion correction was performed in which a two-dimensional rigid realignment was performed independently for each axial slice using the mean image from the first phase of motion correction as the reference image (Cohen-Adad et al., 2009; Weber II et al., 2014). The average temporal signal to noise ratio (tSNR) across the spinal cord was calculated for each phase of motion correction and compared using two-tailed paired t-tests.

2.4 Physiological noise modeling

The cardiac and respiratory cycles are significant sources of noise in spinal cord fMRI and can confound signal detection. To account for this noise, respiratory signals, cardiac signals, and MRI triggers were collected during scanning (sampling rate = 400 Hz, PowerLab 8/30, ADInstruments Inc., Colorado Springs, CO, US), and slice specific voxelwise noise regressors were generated using FSL's physiological noise modeling (PNM) tool, which uses a model-based approach similar to the retrospective image correction (RETROICOR) of physiological motion effects as described by Glover et al. (Brooks et al., 2008; Glover et al., 2000). In brief, a cardiac phase and respiratory phase were assigned to each slice, and the cardiac and respiratory signals were then modeled using a Fourier series (sine and cosine terms) with the principal frequency and the next three harmonics (16 regressors). Multiplicative terms were included to account for the interaction of the cardiac and respiratory cycles (16 additional regressors). A cerebrospinal fluid (CSF) regressor was also generated from the raw CSF signal surrounding the spinal cord using a manually drawn CSF mask. In total, the physiological noise was modeled with 33 regressors, which has been recommended for spinal cord fMRI (Kong et al., 2012). This model does not include the motion parameters as noise regressors, so the effect of including the motion parameters as noise regressors was also explored to control for task-related motion.

2.5 Spatial normalization

Spatial normalization from native space to standard space was performed using the open-source Spinal Cord Toolbox (Cohen-Adad et al., 2014). The structural images of the cervical spine were cropped to include the C2 to T1 vertebrae. The C2 and T1 vertebrae were manually identified, and a vertebral landmarks mask was generated. The functional images

were registered to the structural image using a non-rigid deformation that was constrained to the axial plane (functional to structural registration). The structural images were then straightened along the spinal cord using a binary mask of the spinal cord, and then non-rigid registration to the MNI-Poly-AMU T2-weighted spinal cord template (resolution = 0.5 × 0.5 × 0.5 mm^3) was performed using the vertebral landmarks mask (structural to standard registration) (Fonov et al., 2014). The deformation fields were then concatenated allowing for the forward transformation of the functional images to standard space and the inverse transformation of region of interest (ROI) masks in standard space to native space. The transformed images at each step were visually inspected for quality control. The Spinal Cord Toolbox also contains maps for the vertebral levels and probability maps for the spinal cord segments, which were used to summarize the location of the activity (Cadotte et al., 2015). All reported coordinates are in the MNI-Poly-AMU SC template space.

2.6 Data analysis

At the subject level, the motion-corrected images from each run were concatenated into one 30 min time series, and the spinal cord was extracted from the data using a manually drawn spinal cord mask. Slice-timing correction was then performed, followed by spatial smoothing with a Gaussian kernel of 4 mm full width half maximum (FWHM) and high pass temporal filtering (sigma = 90 s). The task was modeled as a boxcar function with vectors for the left and right components of the task. Statistical maps of the preprocessed times series were generated using FMRIB's Improved Linear Model (FILM) with prewhitening (Woolrich et al., 2001; Worsley, 2001). The design matrix included the hemodynamic response function (gamma, phase 0 s, standard deviation 3 s, average lag 6 s) convolved task vectors as explanatory variables and the temporal derivatives of the task vectors and physiological noise vectors as covariates of no interest. Four contrasts were defined: two for the left and right tasks relative to baseline and two for the difference between the left and right tasks (left > right and right > left). Voxels with a Z-score > 1.65 ($p < 0.05$, uncorrected) were considered active at the subject level. No correction for multiple comparisons was performed at the subject level due to the restricted volume of interrogation as the spinal cord contains a much smaller number of voxels. Furthermore, the presence of false positives was explored through two control analyses (see Control analyses).

For the group analysis, spatial normalization of the statistical images from the subject level analyses to the standard spinal cord template was performed, and average group activation maps for each contrast were generated using FMRIB's Local Analysis of Mixed Effects (FLAME) stages 1 and 2 (Beckmann et al., 2003; Woolrich, 2008; Woolrich et al., 2004). The group average activation maps were thresholded using a Z-score > 1.65 with a cluster significance threshold of $p < 0.05$ (cluster size = 3,669 voxels in standard space, volume = 458.6 mm^3) to correct for multiple comparisons.

In addition to the detection of group and subject level activity, the following analyses were performed:

2.7 Spatial analysis

The number of active voxels in the anterior, posterior, left, and right hemicords at the C4, C5, C6, and C7 vertebral levels was calculated at both the group and subject level for each contrast. Left-right (LR) and anterior-posterior (AP) indices were calculated at the subject level (Seghier, 2008). The indices were calculated by dividing the difference in the number of active voxels between the respective hemicords by the sum (number of active voxels in the entire spinal cord). For the LR index, a value of +1.0 indicates that all active voxels were located in the left hemicord while a value of −1.0 indicates that all active voxels were located in the right hemicord. For the AP index, a value of +1.0 indicates that all active voxels were located in the anterior hemicord while a value of −1.0 indicates that all active voxels were located in the posterior hemicord. To summarize the laterality of the activity across each pair of contrasts, laterality indices were also calculated by taking the median LR index for each pair of contrasts. For the laterality index, a value of +1.0 indicates that all active voxels were located in the hemicord ipsilateral to the task while a value of −1.0 indicates that all active voxels were located in the hemicord contralateral to the task. A Wilcoxon signed-rank test with a hypothesized median of 0 was performed to test for significant localization of the active voxels.

2.8 Peristimulus signal change

Peristimulus time series in percent signal change were generated for the preprocessed data, partial model fit, full model fit, and residuals for the left and right contrasts. The subject level time series were baseline corrected and then averaged across the subjects. The peak signal change of the partial model fit was reported as the peak percent signal change. A two-tailed paired t-test was performed to compare signal change between the left and right contrasts.

2.9 Control analyses

As an additional control for false positives, the task results were compared to two different controls: a task control and a task free control. For the task control, the same 30 minute time series was reanalyzed using randomly generated task vectors with the same constraints as the task (i.e., the same number and duration of the blocks but different order and onset times). For the task free control, the 5 min task free run was analyzed using the task vectors from the first run of the session. For each subject, the number of active voxels and the average Z-score of the active voxels were calculated for each contrast (in standard space), and then the average across each pair of contrasts was calculated. To allow for comparison to the task free control, each run of the task was analyzed separately. The average number of active voxels and the average Z-score of the active voxels for each run were calculated for each contrast, and then the average across the six runs for each pair of contrasts was calculated. Comparisons between the task and control analyses were performed using two-tailed paired t-tests. Group average activation maps were also generated for the task control and the task free control and compared to the properly analyzed group task results.

2.10 Reliability

To investigate the reliability of the activity, the concatenated time series was split, and the first three runs (15 min) and the last three runs (15 min) were analyzed separately. The spatial localization of the activity was assessed at the group and subject level. Intraclass correlation coefficients (ICC) were calculated using the ICC Toolbox to assess the agreement of subject activations from run to run (Caceres et al., 2009). Reliability was then assessed across each of the six runs. A repeated measures analysis of variance was performed to assess for a linear increase or decrease in the number of active voxels and the average Z-score of the active voxels across the runs. For the reliability analyses, the group average activation maps were thresholded at a Zscore > 1.65 with no cluster thresholding.

2.11 Power analysis

To investigate the effect of the length of the time series on the activity, group and subject level analyses were performed on 5, 10, 15, 20, 25, and 30 min of the time series. For each length of the times series, the spatial localization of the activity was assessed, and the number of active voxels and the average Z-score of the active voxels were calculated. Additionally, for each length of data collection, the smallest sample size required for having 80% power was calculated for the hemicord ipsilateral to the task at the C6 vertebral level using fMRI Power (Mumford and Nichols, 2008; Mumford et al., 2007). For the power analysis, the group average activation maps were thresholded at a Z-score > 1.65 with no cluster thresholding.

2.12 Multi-voxel pattern analysis

A trial-wise multi-voxel pattern analysis (MVPA) using a linear support vector machine classifier and leave-onerun- out cross-validation was performed to decode the left and right contrasts based on the activity patterns (Chang and Lin, 2011). The MVPA was performed at each vertebral level. The average accuracy across the subjects was compared to chance (50% accuracy) using one-sample two-tailed t-tests with Bonferroni correction for multiple comparisons.

2.13 Statistical testing

For all non-imaging statistical tests, an $\alpha < 0.05$ was used as the threshold for statistical significance.

3. Results

All subjects successfully completed each run of data collection. No images were excluded due to motion artifacts. Motion correction improved the quality of the data as indicated by the increase in the average tSNR over the spinal cord. The average tSNR ± one SD significantly increased from 10.1 ± 1.7 arbitrary units (au) to 15.4 ± 2.1 au with the first phase of motion correction ($t = 10.763$, $p < 0.001$) and significantly increased from the first phase of motion correction to 16.2 ± 2.1 au with the second phase of motion correction ($t = 9.259$, $p < 0.001$). Following all preprocessing steps (motion correction, slice-timing correction, temporal filtering, spatial smoothing), the average tSNR was 70.2 ± 12.2 au.

Spatial normalization from native space to standard space was successfully performed for each subject, and no data were excluded from the analyses.

3.1 Group level activity

Group spinal cord activity was detected for each of the contrasts as shown in Figure 1 while the task control resulted in no group activity. The left contrast resulted in activity primarily in the left hemicord, and the right contrast resulted in activity primarily in the right hemicord. Activity was more evenly distributed across the anterior and posterior hemicords, and the activity was localized primarily to the C6 vertebral level, which corresponds to the C7 spinal cord segment (Figures 1A and 2A). For the left > right and right > left contrasts, the activity was localized to the hemicord ipsilateral to the task with no activity in the contralateral hemicord. A broader superior-inferior distribution of the activity corresponding to the C5 to C8 spinal cord segments was present for the left > right and right > left contrasts (Figures 1B and 2B). Increasing the threshold to a Z-score > 2.58 ($p < 0.005$) for the left and right contrasts demonstrated activity localized to the ipsilateral anterior quadrant of the spinal cord (Figure 3). The inclusion of the motion parameters as noise regressors in the model (6 parameters or 6 parameters plus their derivatives) or the removal of outliers using FSL's automatic outlier de-weighting had no appreciable effect on the group activity.

3.2 Subject level activity

Spinal cord activity was present for all subjects for each contrast. At the subject level, no significant localization of the activity to the left or right hemicord was present for the left contrast; however, for the right contrast, the activity was significantly localized to the right hemicord. For both the left > right and right > left contrasts, the activity was significantly localized to the hemicord ipsilateral to the task (Table 1A and Supplementary Figure 1A). No significant localization of the activity to the anterior or posterior hemicords was present for any of the contrasts (Table 1B and Supplementary Figure 1B). Increasing the Z-score threshold did not appreciably affect the localization of the activity at the subject level, and no lateralization of the activity was present for the task control or task free control (Table 1C and Supplementary Figure 2).

3.3 Peristimulus signal change

Across the subjects, the average peak signal change ± one between subject SD for the left and right contrasts was 0.49 ± 0.18% and 0.43 ± 0.14%, respectively, with the signal change for the left contrast being significantly higher than the right contrast ($t = 2.259$, $p = 0.047$). The average signal change across time for the remaining residuals was near zero (0.00 ± 0.23% and 0.00 ± 0.15% for the left and right contrasts, respectively) (Supplementary Figure 3).

3.4 Control analyses

3.4.1 Task control—Spinal cord activity was present for all subjects for each contrast for the task and task control (30 min concatenated time series). However, the average number of active voxels ± one SD for the left and right contrasts for the task was 267.1 ± 181.4, which was significantly greater than the task control (171.8 ± 114.2, $t = 2.265$, $p = 0.047$), and the

average Z-score of the active voxels ± one SD for the left and right contrasts for the task was 2.23 ± 0.21, which was significantly greater than the task control (2.09 ± 0.11, t = 2.945, p = 0.015). The number of active voxels for the left > right and right > left contrasts was 233.0 ± 137.9, which was significantly greater than the task control (115.3 ± 39.4, t = 2.923, p = 0.015), and the average Z-score of the active voxels for the left > right and right > left contrasts was 2.21 ± 0.25, which was significantly greater than the task control (2.00 ± 0.09, t = 2.926, p < 0.015). Overall, the spatial extent and magnitude of the activity of the task exceeded that of the task control (Figure 4A).

3.4.2 Task free control—Spinal cord activity was present for all subjects for each contrast for each of the task runs and the task free control run (5 min runs). However, the average number of active voxels across the six runs for the left and right contrasts for the task was 225.2 ± 100.9, which was significantly greater than the task free control (143.7 ± 38.7, t = 2.389, p = 0.038), and the average Z-score of the active voxels across the six runs for the left and right contrasts for the task was 2.17 ± 0.12, which was significantly greater than the task free control (2.08 ± 0.06, t = 2.316, p = 0.043). The average number of active voxels across the six runs for the left > right and right > left contrasts was 238.3 ± 65.9, which was significantly greater than the task free control (159.8 ± 56.3, t = 3.745, p = 0.004), and the average Z-score of the active voxels across the six runs for the left > right and right > left contrasts was 2.22 ± 0.11, which was significantly greater than the task free control (2.08 ± 0.09, t = 2.95, p = 0.014). Overall, the spatial extent and magnitude of the activity of the task exceeded that of the task free control (Figure 4B).

3.5 Reliability

Group activity was present when analyzing the first three runs (15 min) and the last three runs (15 min) separately. At the group and subject level, consistent lateralization of the activity to the ipsilateral hemicord was present for the left > right and right > left contrasts for both 15 min time series (Supplementary Figure 4 and Supplementary Table 1A). The median ICC ± one standard error for the left > right and right > left contrasts were 0.264 ± 0.004 and 0.343 ± 0.007, respectively. Group activity was present for each 5 min run, and consistent lateralization of the activity to the ipsilateral hemicord was present for the left > right and right > left contrasts at the group and subject level for each run (Figure 5A and Supplementary Table 1B). The median ICC across the 5 min runs for the left > right and right > left contrasts were 0.074 ± 0.001 and 0.101 ± 0.002, respectively. No significant linear increase or decrease in the number of active voxels across the runs was present for the left > right (F = 0.435, p = 0.524) or right > left (F = 0.024, p = 0.880) contrasts, and no significant linear increase or decrease in the average Z-score of the active voxels across the runs was present for the left > right (F = 0.791, p = 0.395) or right > left (F = 1.1501, p = 0.347) contrasts.

3.6 Power analysis

Group activity was present for each of the 5, 10, 15, 20, 25, and 30 min time series. Lateralization of the activity was present at the group and subject level for each length of the time series (Figure 5B and Supplementary Table 1C). Based on the group activation maps, the activity appeared to remain consistent after 20 min of data collection. The number of

active voxels and the average Z-score of the active voxels tended to increase with increasing lengths of the time series (Supplementary Figure 5). The number of subjects required for 80% power to detect activity in the ipsilateral hemicord at the C6 vertebral level tended to decrease with increasing lengths of the time series (Figure 5C). At 30 min, the left and right contrasts required 20 and 26 subjects, respectively, for 80% power, while the left > right and right > left contrasts required 13 and 30 subjects, respectively.

3.7 Multi-voxel pattern analysis

MVPA was able to successfully decode the left and right contrasts better than chance at the C6 (average percent accuracy ± one SD = 58.2 ± 6.9%, $t = 3.960$, $\alpha/4 = 0.013$, $p = 0.003$) and C7 (average percent accuracy = 58.2 ± 8.3%, $t = 3.271$, $\alpha/4 = 0.013$, $p = 0.008$) vertebral levels (Figure 6B). Across the C6 to C7 vertebral levels, MVPA was able to decode the left and right contrasts better than chance in the anterior hemicord (average percent accuracy = 58.6 ± 10.3%, $t = 2.755$, $\alpha/2 = 0.025$ $p = 0.020$) and posterior hemicord (average percent accuracy = 57.8 ± 6.6%, $t = 3.963$, $\alpha/2 = 0.025$, $p = 0.003$). MVPA was also able to decode the left and right contrasts better than chance in the left hemicord (average percent accuracy = 58.5 ± 7.2%, $t = 3.910$, $\alpha/2 = 0.025$, $p = 0.003$) but not the right hemicord (average percent accuracy = 55.9 ± 8.3%, $t = 2.361$, $\alpha/2 = 0.025$, $p = 0.039$) (Figure 6C).

4. Discussion

This study demonstrated the feasibility of using fMRI to measure motor-related activity in the cervical spinal cord of healthy subjects at the group and subject level using a left- and right-sided isometric wrist flexion task. The activity exceeded the spatial extent and magnitude of the control analyses, and the activity was anatomically specific and reliable across the runs. The average percent signal change was 0.49 ± 0.18% and 0.43 ± 0.14%, for the left and right contrasts, respectively, which is consistent with previous studies (Giulietti et al., 2008). Further, we were able to use MVPA to decode the left and right contrasts. Based on these reasons, the activity is likely representative of underlying physiological processes and not due to artifact.

Several muscle groups work synergistically to create flexion forces across the wrist. The main wrist flexors are flexor carpi radialis, which receives innervation from the ipsilateral C6 and C7 spinal cord segments, and flexor carpi ulnaris, which receives innervation from the ipsilateral C7 and C8 spinal cord segments. In addition, the tendons of flexor digitorum superficialis (innervation from the ipsilateral C7, C8, and T1 spinal cord segments), palmaris longus (innervation from the ipsilateral C7, C8, and T1 spinal cord segments), and flexor digitorum profundus (innervation from the ipsilateral C8 and T1 spinal cord segments) cross the wrist, and these muscles can also contribute to flexion forces across the wrist. Therefore, contributions from the C6 to T1 spinal cord segments were predicted to contribute to the wrist flexion task (Moore et al., 2014). For the left and right contrasts, the group activity was localized primarily to the C7 spinal cord segment. For the left > right and right > left contrasts, the group activity had a broader superior-inferior distribution extending across the C5 to C8 spinal cord segments. Activity in the C5 spinal cord segment was not expected and

may be due to some coactivation of the arm and shoulder muscles to stabilize the upper extremity during force production across the wrist (Osu and Gomi, 1999). The lack of activity in the T1 spinal cord segment suggests that the contribution from the T1 spinal cord segment was less or absent. Future studies could include multi-channel electromyography (EMG) measurements in order to disentangle the contributions of the different muscle groups to the activity in the different spinal cord segments. The broader superior-inferior distribution of the activity for the left > right and right > left contrasts may demonstrate that modeling the difference between the tasks was more sensitive than modeling the tasks relative to baseline. Previous spinal cord fMRI motor studies have only modeled the task relative to baseline.

The major finding was that the activity was lateralized to the hemicord ipsilateral to the task, which is consistent with the present understanding of the anatomy and function of the spinal cord. The ipsilateral anterior activity likely represents motoneuron activity. The motoneuron cell bodies responsible for wrist flexion are located in the ipsilateral anterior horn of the spinal cord within the C6 to T1 spinal cord segments (Moore et al., 2014), and their activation by descending inputs is required for voluntary force production across the wrist (Tansey and Botterman, 1996). The ipsilateral posterior activity likely represents task-related sensory input into the cord. Muscle contraction and force production across the wrist results in the activation of cutaneous, joint, and muscle afferents, which largely synapse in the ipsilateral anterior and posterior horns of the spinal cord at the same spinal segments (Bessou et al., 1986). For the left and right contrasts, the group activity was localized primarily to the hemicord ipsilateral to the motor task. Some activity extended into the contralateral hemicord, and the overlap of activity was mainly in the intermediate zone of the spinal cord. The overlap of activity may represent areas of combined neural processing for both the left and right tasks as descending projections from the primary motor cortex have been shown to synapse in the intermediate zone of the ipsilateral and contralateral hemicords in primates (Kuypers and Brinkman, 1970). The overlap may also be an artifact as a result of spatial smoothing. In this study, a 4 mm FWHM 3D Gaussian kernel was used for smoothing. In a preliminary analysis, this level of smoothing was determined to be optimal to smooth across the slices (slice thickness = 3 mm). A future study will explore the effect of different smoothing parameters on the spatial extent, magnitude, and location of the activity in the spinal cord. For the left > right and right > left contrasts, the activity was localized entirely to the hemicord ipsilateral to the motor task with no activity in the contralateral hemicord. Based on this finding, the areas of overlap for the left and right contrasts were approximately equal in signal change when compared to baseline.

With the *a priori* levels of significance, no significant localization of the activity to the anterior or posterior hemicord was present at the group or subject level. When increasing the significance threshold (decreasing the p-value) at the group level, the activity was localized to the ipsilateral anterior quadrant of the spinal cord, which suggests that the signal change from motoneuron activity was greater than that of the sensory input. At the subject level, increasing the significance threshold level resulted in some subjects having no significant activity and did not appreciably affect the AP localization of the signal.

For the left > right and right > left contrasts, the lateralization of the activity to the ipsilateral hemicord was present for both 15 min time series and across each of the 5 min runs at both the group and subject level. Despite the reliability of the lateralization, the superior-inferior distribution of the group activity varied accounting for the low ICC between the 15 min time series and the even lower ICC across the 5 min runs. Greater consistency of the activity was expected, and overall, the underlying reason for the variability is unknown. The number of active voxels and the average Z-score of the active voxels did not significantly increase or decrease across the runs, and no subjects reported fatigue from the task. Perhaps, the subjects varied their flexion force or motor control strategy across the runs, as multiple muscles can produce flexion forces across the wrist. Considering this hypothesis, the boxcar model may be insufficient to account for the variability in the force output or motor control strategy across the runs, and possibly modeling the fMRI signal using the wrist flexion force or EMG signals from multiple muscles would account for this variability and result in more stable activation maps across the runs.

Our results support the findings of the study by Maerion et al. (Maieron et al., 2007). In this study, thirteen healthy subjects performed a left or right thumb to finger apposition task in a block design. The left or right tasks were compared to baseline, and the number of active voxels for the task was compared to a task free control similar to the current study. No spatial normalization of the subject level analyses was performed, so no group average activation maps were generated. The findings from the study demonstrated that the number of active voxels during the task significantly exceeded that of the control and the activity was lateralized to the hemicord ipsilateral to the task across the subjects. For the spatial analysis, the study used the total number of active voxels in each hemicord and made comparisons with paired t-tests. In comparison, the current study calculated LR indices, which normalized the location of the activity based on each subjects overall activity level. We found that the distribution of the LR indices was not normal so non-parametric tests were used in this study. The differences in methods may account for the lack of significant localization of the activity to the left hemicord for the left contrast in the current study.

The general linear model uses an encoding model to determine the pattern of activity given the experimental conditions (i.e., left- or right-sided motor task). In contrast, MVPA uses a decoding model to determine the likelihood of the experimental conditions given the pattern of activity (Naselaris et al., 2011). In this study, both encoding and decoding analyses were employed. Not only were we able to demonstrate the lateralization of the spinal cord activity using an encoding model, but we were also successfully able to use a decoding model to determine the likelihood of the experimental conditions given the pattern of activity. While the overall accuracy of the decoding model was low, the results demonstrated that sufficient information was present in the pattern of spinal cord activity to successfully decode the experimental conditions.

In this study, we used the ZOOMit selective field-of-view imaging sequence on a 3.0 T Siemens Prisma MR scanner. Specifically, the sequence uses a parallel transmit system to only excite the volume of interest. This allows the use of a reduced field-of-view while preventing aliasing. The reduced field-of-view decreases the number of phase encoding

steps, which allowed for high resolution imaging ($1.0 \times 1.0 \times 3.0$ mm^3) of the entire cervical spinal cord enlargement with a sampling period of 2.5 s in this study.

Few spinal cord fMRI studies have spatially normalized the subject level analyses to a standard space template to allow for the generation of group activation maps (Brooks et al., 2012; Cahill and Stroman, 2011; Eippert et al., 2009). In this study, the Spinal Cord Toolbox was used for spatial normalization; the Spinal Cord Toolbox is an open source software package specifically designed for spinal cord imaging (Cohen-Adad et al., 2014; Fonov et al., 2014). The toolbox allowed for robust normalization of the subject level analyses to a standard template, which likely had a major contribution to the significant group activity and spatial localization of the activity in this study. Despite the robust normalization to the template, much across subject variation exists in the location of the spinal cord segments in relation to the vertebral bodies (Cadotte et al., 2015). The effects of this variation on the present results are unknown. Accounting for this variation with more advanced normalization algorithms should allow for even more robust and accurate group analyses along the superior-inferior axis.

The majority of spinal cord fMRI studies have attempted to detect activity from sensory stimulation. While spinal cord fMRI has much potential for studying sensory processing, several factors can influence sensory processing in the spinal cord (e.g., adaptation and sensitization), and these factors could potentially complicate the fMRI signal in the spinal cord influencing its detection and interpretation (Andrew and Greenspan, 1999; Bensmaia et al., 2005). Motor studies on the other hand may provide a more optimal experimental paradigm for further characterizing the signal in spinal cord fMRI because the motoneuron activity can be measured noninvasively by taking force and EMG measures (De Luca et al., 1982; Henneman et al., 1965; Lippold, 1952). Future studies could model the spinal cord signal using the force and EMG measures to more robustly detect motoneuron activity.

5. Conclusion

We were able to robustly detect cervical spinal cord activity at the group and subject level. The activity was lateralized to the ipsilateral hemicord, and the activity was reliable.

Supplementary Material

Refer to Web version on PubMed Central for supplementary material.

Acknowledgements

Research reported in this publication was supported by the National Center For Complementary and Integrative Health under award number F32AT007800 and the National Institute of Child Health and Development under award number T32HD057845. The content is solely the responsibility of the authors and does not necessarily represent the official views of the National Institutes of Health.

Abbreviations

BOLD blood oxygen level dependent

MR	magnetic resonance
MRI	magnetic resonance imaging
fMRI	functional magnetic resonance imaging
SPACE	Sampling perfection with application optimized contrast using different flip angle evolutions
FMRIB	Oxford Center for Functional MRI of the Brain
FSL	FMRIB's Software Library
PNM	physiological noise modeling

References

Andrew D, Greenspan JD. Mechanical and heat sensitization of cutaneous nociceptors after peripheral inflammation in the rat. J Neurophysiol. 1999; 82:2649–2656. [PubMed: 10561434]

Backes WH, Mess WH, Wilmink JT. Functional MR imaging of the cervical spinal cord by use of median nerve stimulation and fist clenching. AJNR Am J Neuroradiol. 2001; 22:1854–1859. [PubMed: 11733315]

Bandettini PA, Wong EC, Hinks RS, Tikofsky RS, Hyde JS. Time course EPI of human brain function during task activation. Magn Reson Med. 1992; 25:390–397. [PubMed: 1614324]

Beckmann CF, Jenkinson M, Smith SM. General multilevel linear modeling for group analysis in FMRI. Neuroimage. 2003; 20:1052–1063. [PubMed: 14568475]

Bensmaia SJ, Leung YY, Hsiao SS, Johnson KO. Vibratory adaptation of cutaneous mechanoreceptive afferents. J Neurophysiol. 2005; 94:3023–3036. [PubMed: 16014802]

Bessou P, Cabelguen JM, Joffroy M, Montoya R, Pages B. Efferent and afferent activity in a gastrocnemius nerve branch during locomotion in the thalamic cat. Exp Brain Res. 1986; 64:553–568. [PubMed: 2948830]

Bouwman CJ, Wilmink JT, Mess WH, Backes WH. Spinal cord functional MRI at 3 T: gradient echo echo-planar imaging versus turbo spin echo. Neuroimage. 2008; 43:288–296. [PubMed: 18706507]

Brooks JC, Beckmann CF, Miller KL, Wise RG, Porro CA, Tracey I, Jenkinson M. Physiological noise modelling for spinal functional magnetic resonance imaging studies. Neuroimage. 2008; 39:680–692. [PubMed: 17950627]

Brooks JC, Kong Y, Lee MC, Warnaby CE, Wanigasekera V, Jenkinson M, Tracey I. Stimulus site and modality dependence of functional activity within the human spinal cord. J Neurosci. 2012; 32:6231–6239. [PubMed: 22553029]

Caceres A, Hall DL, Zelaya FO, Williams SC, Mehta MA. Measuring fMRI reliability with the intra-class correlation coefficient. Neuroimage. 2009; 45:758–768. [PubMed: 19166942]

Cadotte DW, Cadotte A, Cohen-Adad J, Fleet D, Livne M, Wilson JR, Mikulis D, Nugaeva N, Fehlings MG. Characterizing the location of spinal and vertebral levels in the human cervical spinal cord. AJNR Am J Neuroradiol. 2015; 36:803–810. [PubMed: 25523587]

Cahill CM, Stroman PW. Mapping of neural activity produced by thermal pain in the healthy human spinal cord and brain stem: a functional magnetic resonance imaging study. Magn Reson Imaging. 2011; 29:342–352. [PubMed: 21247717]

Chang C-C, Lin C-J. LIBSVM: A library for support vector machines. ACM Trans. Intell. Syst. Technol. 2011; 2:1–27.

Cincotta M, Ziemann U. Neurophysiology of unimanual motor control and mirror movements. Clin Neurophysiol. 2008; 119:744–762. [PubMed: 18187362]

Cohen-Adad, J.; De Leener, B.; Benhamou, M.; Lévy, S.; Touati, J.; Cadotte, D.; Fleet, D.; Cadotte, A.; Fehlings, M.; Pelletier Paquette, JP.; Thong, W.; Taso, M.; Collins, L.; Callot, V.; Fonov, V.

Spinal Cord Toolbox: an open-source framework for processing spinal cord MRI data. 20th Annual Meeting of the Organization for Human Brain Mapping; Hamburg, Germany. 2014.

Cohen-Adad, J.; Rossignol, S.; Hoge, RD. Slice-by-slice motion correction in spinal cord fMRI: SliceCorr. Proceedings of the 17th Annual Meeting of the International Society for Magnetic Resonance in Medicine; Honolulu, USA. 2009.

De Luca CJ, LeFever RS, McCue MP, Xenakis AP. Behaviour of human motor units in different muscles during linearly varying contractions. J Physiol. 1982; 329:113–128. [PubMed: 7143246]

Eippert F, Finsterbusch J, Bingel U, Buchel C. Direct evidence for spinal cord involvement in placebo analgesia. Science. 2009; 326:404. [PubMed: 19833962]

Fonov VS, Le Troter A, Taso M, De Leener B, Leveque G, Benhamou M, Sdika M, Benali H, Pradat PF, Collins DL, Callot V, Cohen-Adad J. Framework for integrated MRI average of the spinal cord white and gray matter: the MNI-Poly-AMU template. Neuroimage. 2014; 102(Pt 2):817–827. [PubMed: 25204864]

Fratini M, Moraschi M, Maraviglia B, Giove F. On the impact of physiological noise in spinal cord functional MRI. J Magn Reson Imaging. 2014; 40:770–777. [PubMed: 24925698]

Giulietti G, Giove F, Garreffa G, Colonnese C, Mangia S, Maraviglia B. Characterization of the functional response in the human spinal cord: Impulse-response function and linearity. Neuroimage. 2008; 42:626–634. [PubMed: 18599318]

Glover GH, Li TQ, Ress D. Image-based method for retrospective correction of physiological motion effects in fMRI: RETROICOR. Magn Reson Med. 2000; 44:162–167. [PubMed: 10893535]

Govers N, Beghin J, Van Goethem JW, Michiels J, van den Hauwe L, Vandervliet E, Parizel PM. Functional MRI of the cervical spinal cord on 1.5 T with fingertapping: to what extent is it feasible? Neuroradiology. 2007; 49:73–81. [PubMed: 17119948]

Henneman E, Somjen G, Carpenter DO. Excitability and inhibitability of motoneurons of different sizes. J Neurophysiol. 1965; 28:599–620. [PubMed: 5835487]

Jenkinson M, Bannister P, Brady M, Smith S. Improved optimization for the robust and accurate linear registration and motion correction of brain images. Neuroimage. 2002; 17:825–841. [PubMed: 12377157]

Jenkinson M, Beckmann CF, Behrens TE, Woolrich MW, Smith SM. FSL. Neuroimage. 2012; 62:782–790. [PubMed: 21979382]

Jenny AB, Inukai J. Principles of motor organization of the monkey cervical spinal cord. J Neurosci. 1983; 3:567–575. [PubMed: 6827309]

Joliot M, Papathanassiou D, Mellet E, Quinton O, Mazoyer N, Courtheoux P, Mazoyer B. FMRI and PET of self-paced finger movement: comparison of intersubject stereotaxic averaged data. Neuroimage. 1999; 10:430–447. [PubMed: 10493901]

Kim SG, Ashe J, Hendrich K, Ellermann JM, Merkle H, Ugurbil K, Georgopoulos AP. Functional magnetic resonance imaging of motor cortex: hemispheric asymmetry and handedness. Science. 1993; 261:615–617. [PubMed: 8342027]

Komisaruk BR, Mosier KM, Liu WC, Criminale C, Zaborszky L, Whipple B, Kalnin A. Functional localization of brainstem and cervical spinal cord nuclei in humans with fMRI. AJNR Am J Neuroradiol. 2002; 23:609–617. [PubMed: 11950653]

Kong Y, Jenkinson M, Andersson J, Tracey I, Brooks JC. Assessment of physiological noise modelling methods for functional imaging of the spinal cord. Neuroimage. 2012; 60:1538–1549. [PubMed: 22178812]

Kornelsen J, Stroman PW. fMRI of the lumbar spinal cord during a lower limb motor task. Magn Reson Med. 2004; 52:411–414. [PubMed: 15282826]

Kornelsen J, Stroman PW. Detection of the neuronal activity occurring caudal to the site of spinal cord injury that is elicited during lower limb movement tasks. Spinal Cord. 2007; 45:485–490. [PubMed: 17245349]

Kuypers HG, Brinkman J. Precentral projections to different parts of the spinal intermediate zone in therhesus monkey. Brain Res. 1970; 24:29–48. [PubMed: 4099987]

Kwong KK, Belliveau JW, Chesler DA, Goldberg IE, Weisskoff RM, Poncelet BP, Kennedy DN, Hoppel BE, Cohen MS, Turner R, et al. Dynamic magnetic resonance imaging of human brain

activity during primary sensory stimulation. Proc Natl Acad Sci U S A. 1992; 89:5675–5679. [PubMed: 1608978]

Lemon RN, Griffiths J. Comparing the function of the corticospinal system in different species: organizational differences for motor specialization? Muscle Nerve. 2005; 32:261–279. [PubMed: 15806550]

Lichy MP, Wietek BM, Mugler JP 3rd, Horger W, Menzel MI, Anastasiadis A, Siegmann K, Niemeyer T, Konigsrainer A, Kiefer B, Schick F, Claussen CD, Schlemmer HP. Magnetic resonance imaging of the body trunk using a single-slab, 3-dimensional, T2-weighted turbo-spin-echo sequence with high sampling efficiency (SPACE) for high spatial resolution imaging: initial clinical experiences. Invest Radiol. 2005; 40:754–760. [PubMed: 16304477]

Lippold OC. The relation between integrated action potentials in a human muscle and its isometric tension. J Physiol. 1952; 117:492–499. [PubMed: 12991236]

Madi S, Flanders AE, Vinitski S, Herbison GJ, Nissanov J. Functional MR imaging of the human cervical spinal cord. AJNR Am J Neuroradiol. 2001; 22:1768–1774. [PubMed: 11673177]

Maehara M, Ikeda K, Kurokawa H, Ohmura N, Ikeda S, Hirokawa Y, Maehara S, Utsunomiya K, Tanigawa N, Sawada S. Diffusion-weighted echo-planar imaging of the head and neck using 3-T MRI: Investigation into the usefulness of liquid perfluorocarbon pads and choice of optimal fat suppression method. Magn Reson Imaging. 2014; 32:440–445. [PubMed: 24582547]

Maieron M, Iannetti GD, Bodurka J, Tracey I, Bandettini PA, Porro CA. Functional responses in the human spinal cord during willed motor actions: evidence for side- and rate-dependent activity. J Neurosci. 2007; 27:4182–4190. [PubMed: 17428996]

Moore KL, Dalley AF, Agur AMR. Clinically oriented anatomy. 2014

Mugler JP 3rd, Bao S, Mulkern RV, Guttmann CR, Robertson RL, Jolesz FA, Brookeman JR. Optimized single-slab three-dimensional spin-echo MR imaging of the brain. Radiology. 2000; 216:891–899. [PubMed: 10966728]

Mumford JA, Nichols TE. Power calculation for group fMRI studies accounting for arbitrary design and temporal autocorrelation. Neuroimage. 2008; 39:261–268. [PubMed: 17919925]

Mumford, JA.; Poldrack, R.; Nichols, T. FMRIpower: A Power Calculation Tool for 2-Stage fMRI models. 13th Annual Meeting of the Organization for Human Brain Mapping; Chicago, USA. 2007.

Naselaris T, Kay KN, Nishimoto S, Gallant JL. Encoding and decoding in fMRI. Neuroimage. 2011; 56:400–410. [PubMed: 20691790]

Ng MC, Wong KK, Li G, Lai S, Yang ES, Hu Y, Luk KD. Proton-density-weighted spinal fMRI with sensorimotor stimulation at 0.2 T. Neuroimage. 2006; 29:995–999. [PubMed: 16140548]

Ng MC, Wu EX, Lau HF, Hu Y, Lam EY, Luk KD. Cervical spinal cord BOLD fMRI study: modulation of functional activation by dexterity of dominant and non-dominant hands. Neuroimage. 2008; 39:825–831. [PubMed: 17962042]

Osu R, Gomi H. Multijoint muscle regulation mechanisms examined by measured human arm stiffness and EMG signals. J Neurophysiol. 1999; 81:1458–1468. [PubMed: 10200182]

Pfeuffer J, van de Moortele PF, Yacoub E, Shmuel A, Adriany G, Andersen P, Merkle H, Garwood M, Ugurbil K, Hu X. Zoomed functional imaging in the human brain at 7 Tesla with simultaneous high spatial and high temporal resolution. Neuroimage. 2002; 17:272–286. [PubMed: 12482083]

Rieseberg S, Frahm J, Finsterbusch J. Two-dimensional spatially-selective RF excitation pulses in echo-planar imaging. Magn Reson Med. 2002; 47:1186–1193. [PubMed: 12111965]

Seghier ML. Laterality index in functional MRI: methodological issues. Magn Reson Imaging. 2008; 26:594–601. [PubMed: 18158224]

Smith SM, Jenkinson M, Woolrich MW, Beckmann CF, Behrens TE, Johansen-Berg H, Bannister PR, De Luca M, Drobnjak I, Flitney DE, Niazy RK, Saunders J, Vickers J, Zhang Y, De Stefano N, Brady JM, Matthews PM. Advances in functional and structural MR image analysis and implementation as FSL. Neuroimage. 2004; 23(Suppl 1):S208–S219. [PubMed: 15501092]

Stroman PW, Krause V, Malisza KL, Frankenstein UN, Tomanek B. Characterization of contrast changes in functional MRI of the human spinal cord at 1.5 T. Magn Reson Imaging. 2001; 19:833–838. [PubMed: 11551724]

Stroman PW, Nance PW, Ryner LN. BOLD MRI of the human cervical spinal cord at 3 tesla. Magn Reson Med. 1999; 42:571–576. [PubMed: 10467302]

Stroman PW, Ryner LN. Functional MRI of motor and sensory activation in the human spinal cord. Magn Reson Imaging. 2001; 19:27–32. [PubMed: 11295343]

Stroman PW, Wheeler-Kingshott C, Bacon M, Schwab JM, Bosma R, Brooks J, Cadotte D, Carlstedt T, Ciccarelli O, Cohen-Adad J, Curt A, Evangelou N, Fehlings MG, Filippi M, Kelley BJ, Kollias S, Mackay A, Porro CA, Smith S, Strittmatter SM, Summers P, Tracey I. The current state-of-theart of spinal cord imaging: methods. Neuroimage. 2014; 84:1070–1081. [PubMed: 23685159]

Tansey KE, Botterman BR. Activation of type-identified motor units during centrally evoked contractions in the cat medial gastrocnemius muscle. I. Motor-unit recruitment. J Neurophysiol. 1996; 75:26–37. [PubMed: 8822539]

Vahdat S, Lungu O, Cohen-Adad J, Marchand-Pauvert V, Benali H, Doyon J. Simultaneous Brain-Cervical Cord fMRI Reveals Intrinsic Spinal Cord Plasticity during Motor Sequence Learning. PLoS Biol. 2015; 13:e1002186. [PubMed: 26125597]

van Gelderen P, Ramsey NF, Liu G, Duyn JH, Frank JA, Weinberger DR, Moonen CT. Three-dimensional functional magnetic resonance imaging of human brain on a clinical 1.5-T scanner. Proc Natl Acad Sci U S A. 1995; 92:6906–6910. [PubMed: 7624341]

Weber, KA., II; Chen, Y.; Wang, X.; Parrish, TB. Choice of Motion Correction Method Affects Spinal Cord fMRI Results. 20th Annual Meeting of the Organization for Human Brain Mapping; Hamburg, Germany. 2014.

Woolrich M. Robust group analysis using outlier inference. Neuroimage. 2008; 41:286–301. [PubMed: 18407525]

Woolrich MW, Behrens TE, Beckmann CF, Jenkinson M, Smith SM. Multilevel linear modelling for FMRI group analysis using Bayesian inference. Neuroimage. 2004; 21:1732–1747. [PubMed: 15050594]

Woolrich MW, Ripley BD, Brady M, Smith SM. Temporal autocorrelation in univariate linear modeling of FMRI data. Neuroimage. 2001; 14:1370–1386. [PubMed: 11707093]

Worsley, KJ. Statistical analysis of activation images. In: Jezzard, P.; Matthews, PM.; Smith, SM., editors. Functional MRI: An Introduction to Methods. USA: Oxford University Press; 2001.

Xie CH, Kong KM, Guan JT, Chen YX, He JK, Qi WL, Wang XJ, Shen ZW, Wu RH. SSFSE sequence functional MRI of the human cervical spinal cord with complex finger tapping. Eur J Radiol. 2009; 70:1–6. [PubMed: 18353589]

Yoshizawa T, Nose T, Moore GJ, Sillerud LO. Functional magnetic resonance imaging of motor activation in the human cervical spinal cord. Neuroimage. 1996; 4:174–182. [PubMed: 9345507]

Highlights

- fMRI was used to detect motor-related activity in the cervical spinal cord
- Subjects performed a left- and right-sided isometric wrist flexion task
- Significant activity was detected and exceeded the control analyses
- Activity was lateralized to the ipsilateral hemicord at the group and subject level
- The lateralization was reliable across the runs at the group and subject level

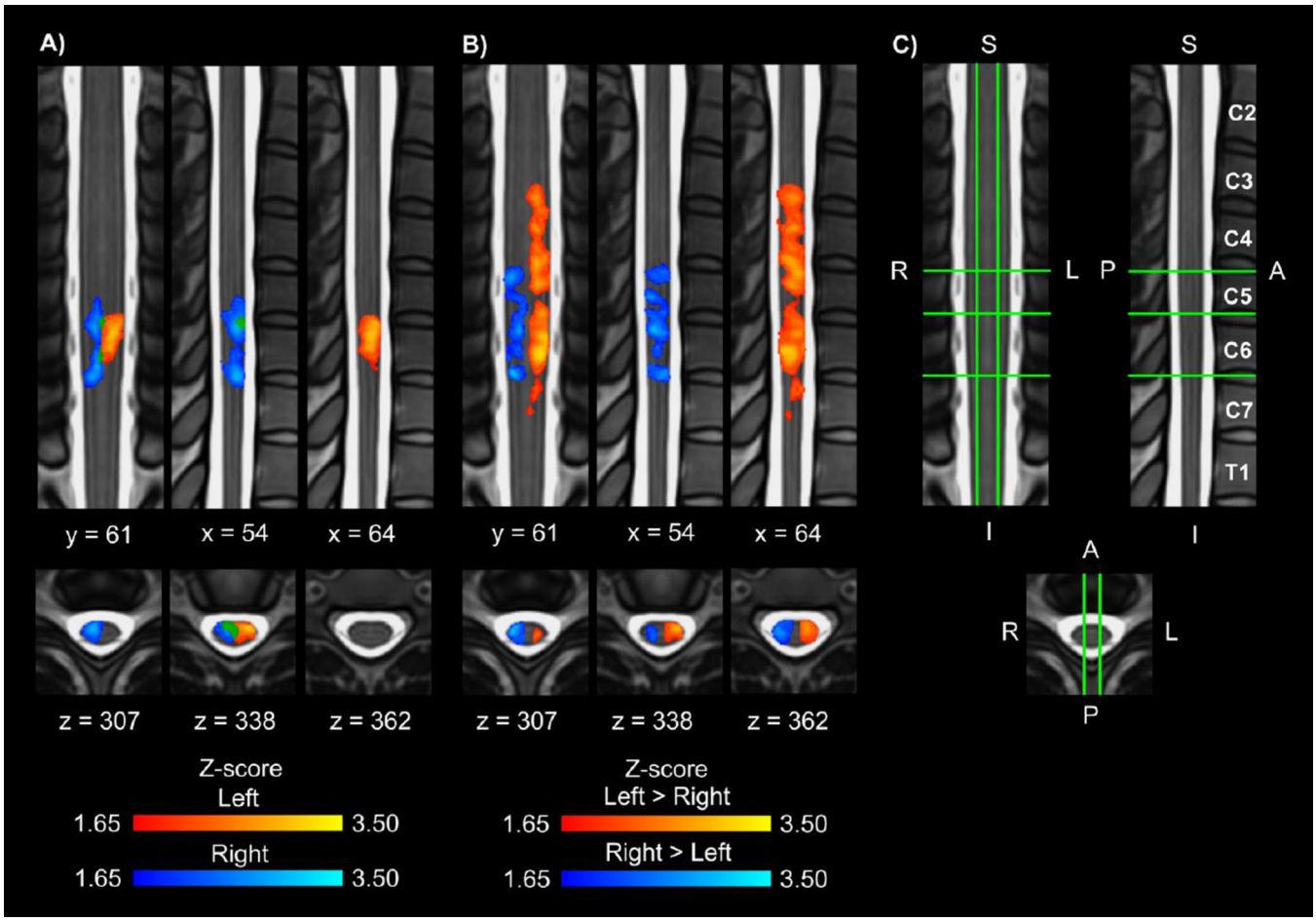

Figure 1.

A) Group average activation maps (1 coronal, 2 sagittal, and 3 axial slices) resulting from the left (red-yellow) and right (blue-light blue) contrasts (overlap in green). B) Group average activation maps (1 coronal, 2 sagittal, and 3 axial slices) for the left > right (red-yellow) and right > left (blue-light blue) contrasts. For A and B, the average activation maps were thresholded at a Z-score > 1.65 with a cluster threshold of $p < 0.05$ to correct for multiple comparisons. The task control resulted in no group activity at this threshold. C) Legend showing location of the coronal, sagittal, and axial slices on the standard spinal cord template with the corresponding vertebrae labeled. The location of the slices shown remains constant across all figures. L = left, R = right, S = superior, I = inferior, A = anterior, P = posterior.

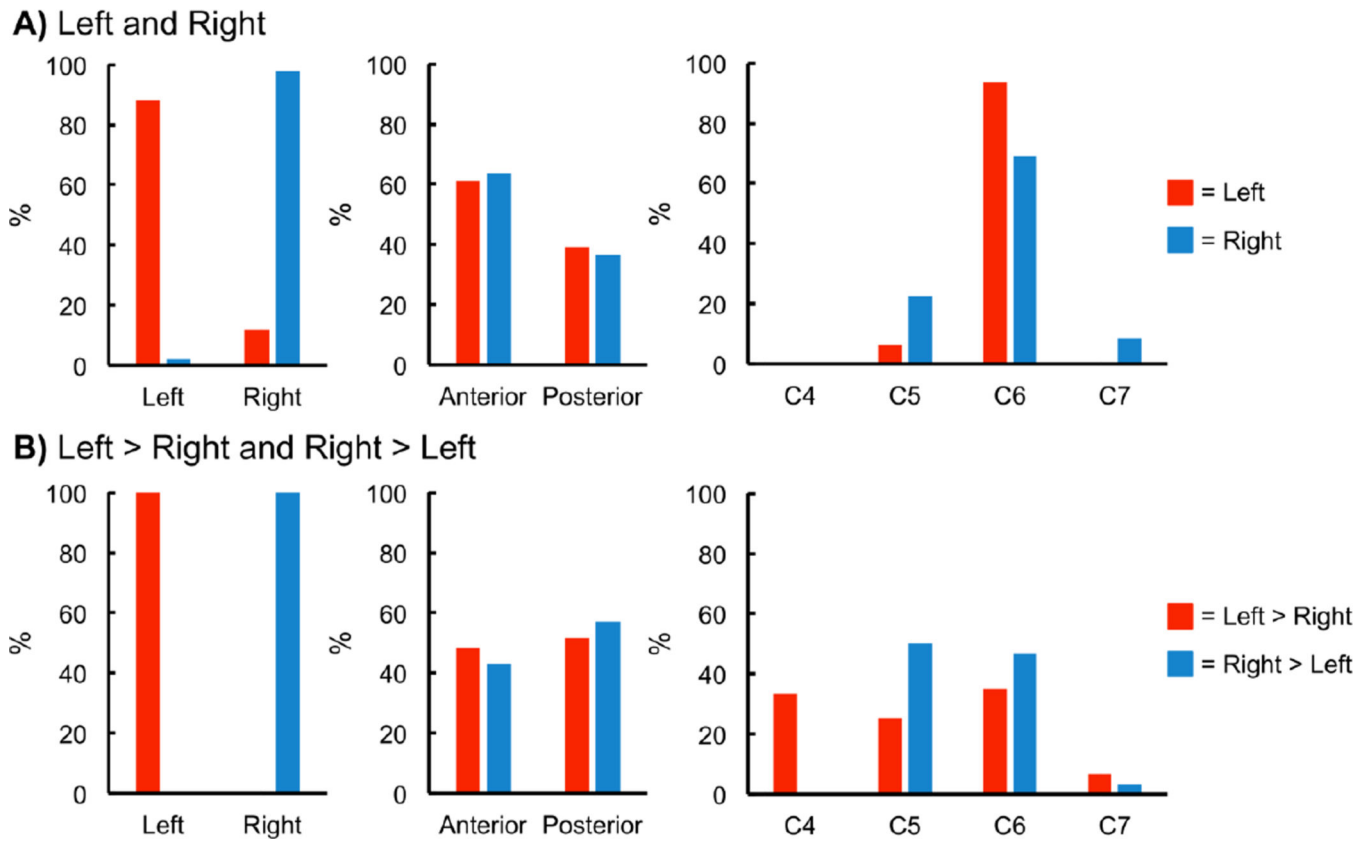

Figure 2.

Location of the group average activity shown in Figure 1. A) The left contrast resulted in activity primarily in the left hemicord, and the right contrast resulted in activity primarily in the right hemicord. Activity was more evenly distributed across the anterior and posterior hemicords. In the superior-inferior direction the activity was localized primarily to the C6 vertebral level, which corresponds to the C7 spinal cord segment. B) For the left > right and right > left contrasts, the activity was localized to the hemicord ipsilateral to the task with no activity in the contralateral hemicord. A broader superior-inferior distribution of the activity was also present. % = percentage of the active voxels located in the corresponding hemicord or vertebral level.

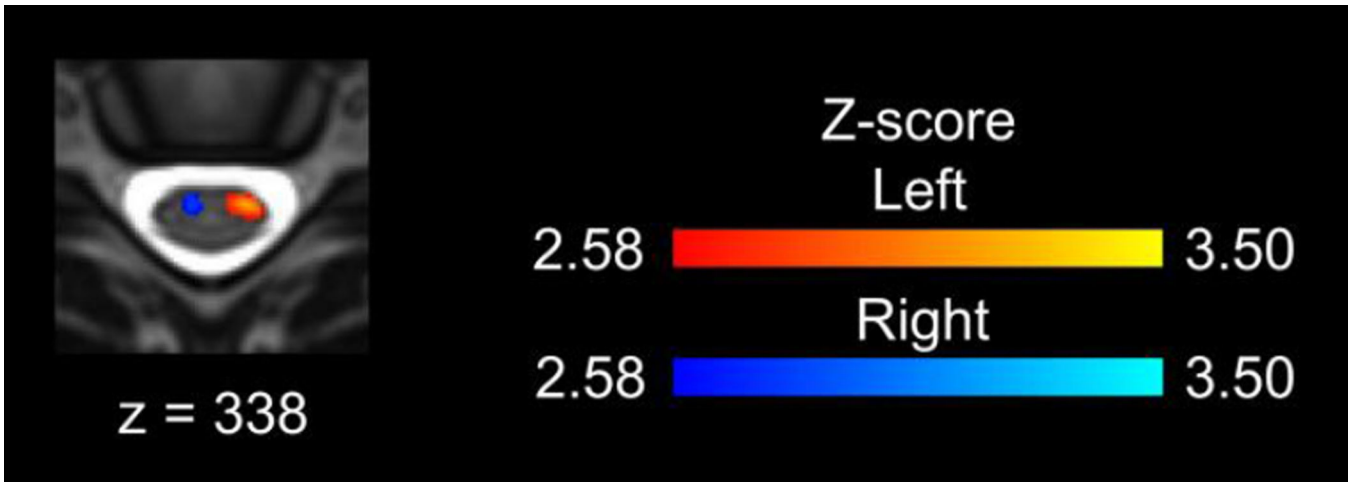

Figure 3.
Increasing the threshold on the group average activation maps to a Z-score of 2.58 ($p < 0.005$) resulted in activity localized to the ipsilateral anterior quadrant of the spinal cord.

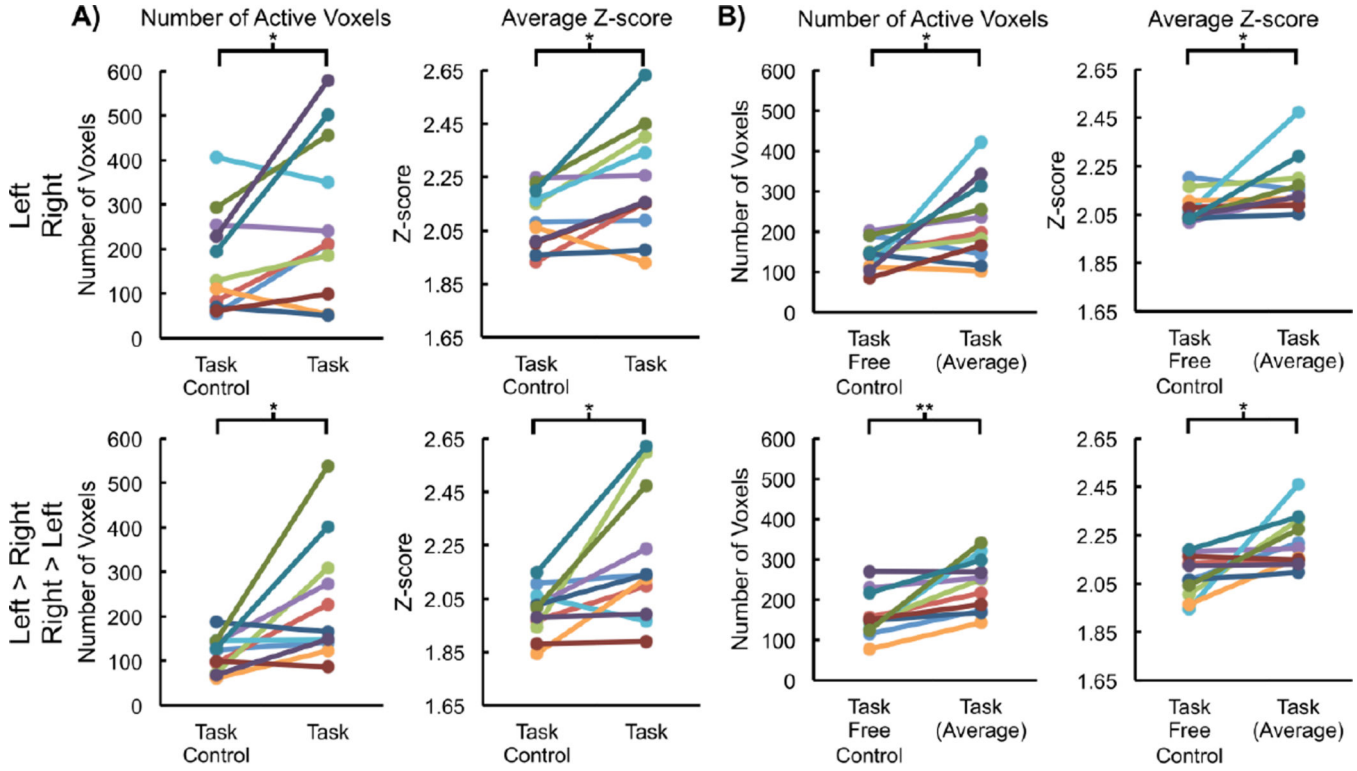

Figure 4.

For the task, task control, and task free control, the number of active voxels and the average Z-score of the active voxels were calculated for each subject and compared as a control for false positives. The task resulted in more active voxels with a greater average Z-score than both the task control (A) and task free control (B). *$p < 0.05$ and **$p < 0.01$.

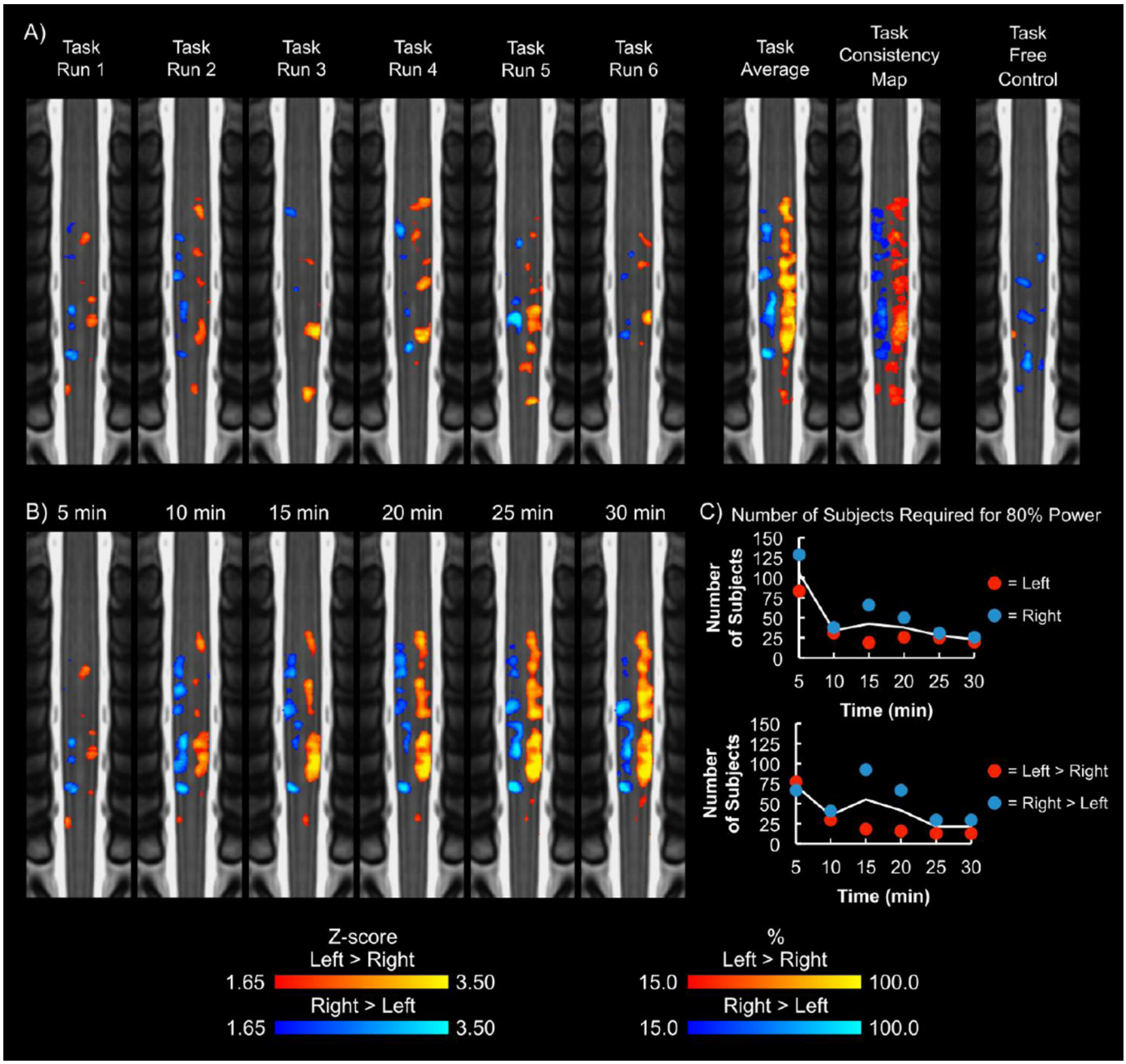

Figure 5.

A) Group average activation maps (coronal slices) for each run of the task for the left > right (yellow-red) and right > left (blue-light blue) contrasts. For each run of the task, the activity was primarily localized to the hemicord ipsilateral to the task. The average group activity and consistency maps across the six runs were calculated for comparison. The average group activity and consistency maps demonstrated lateralization of the activity to the corresponding hemicord. In comparison, the task free control resulted in areas of activity, but the activity was not localized to a specific region of the spinal cord. The activation maps were thresholded at a Zscore > 1.65 with no cluster thresholding. The task consistency map shows the percentage of the six task runs that a voxel was active. B) Group average

activation maps for increasing lengths of the time series are shown. Overall, the activity detected appears to remain consistent after 20 min of data collection. The group average activation maps were thresholded at a Z-score > 1.65 with no cluster thresholding. C) The number of subjects required for 80% power to detect activity in the ipsilateral hemicord at the C6 vertebral level was calculated for each time series length. The solid line represents the average of the contrasts. At 30 min, the left and right contrasts required 20 and 26 subjects, respectively, for 80% power, while the left > right and right > left contrasts required 13 and 30 subjects, respectively.

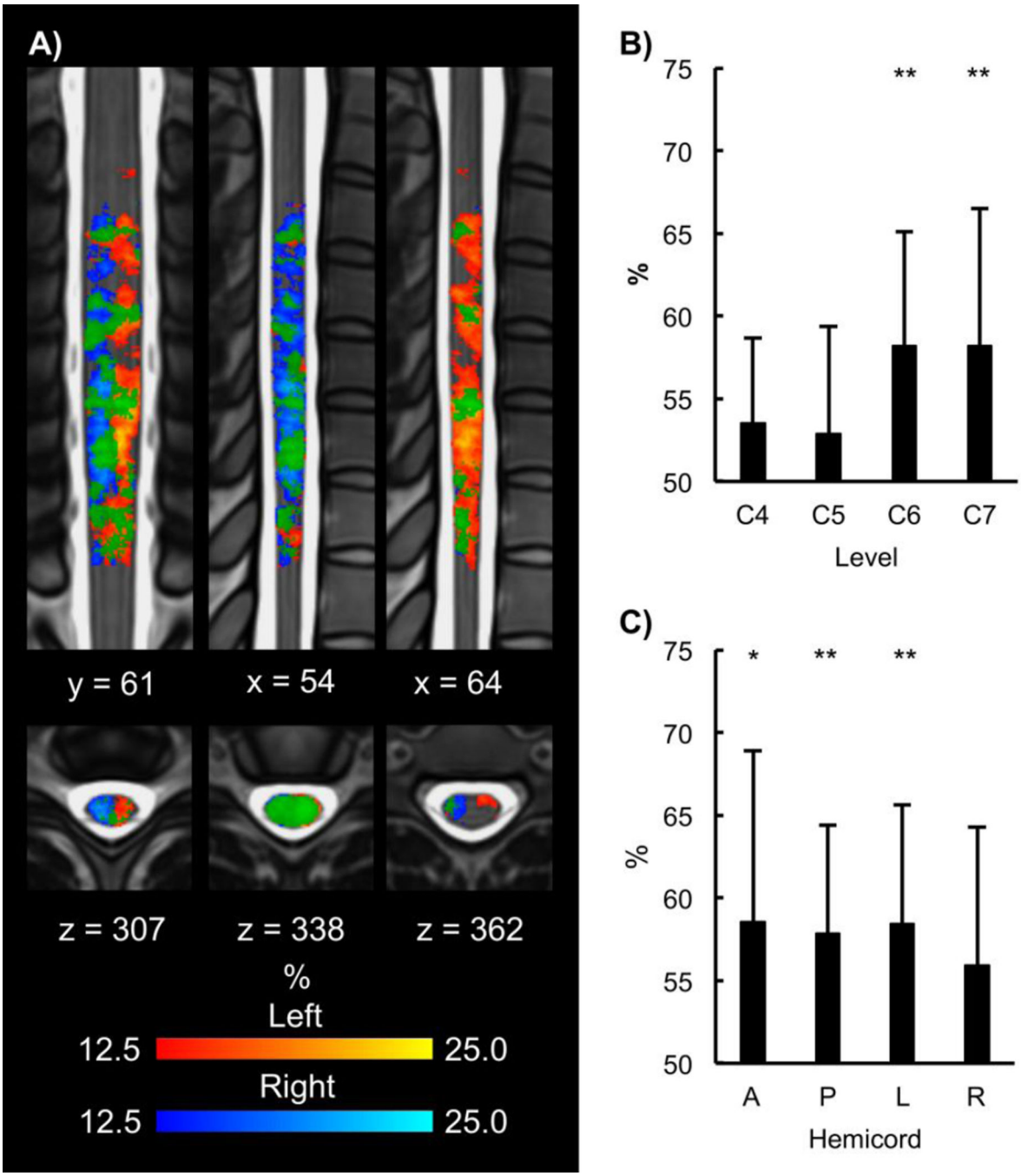

Figure 6.

A) Across subject trialwise consistency maps (1 coronal, 2 sagittal, and 3 axial slices) for the left (yellow-red) and right (blue-light blue) contrasts (overlap in green). The consistency maps show the percentage across all trials and all subjects that a voxel was active (Zscore > 1.65). Overall, the consistency maps demonstrate lateralization of the activity to the hemicord ipsilateral to the task at the trial level. B) Percent accuracy of the trialwise multi-voxel pattern analysis (MVPA) at each vertebral level is shown. MVPA was able to decode the left and right contrasts at the C6 and C7 vertebral levels better than chance. C) Trialwise

MVPA was then performed across the C6 to C7 vertebral levels in the anterior, posterior, left, and right hemicords. At C6 to C7, MVPA was able to decode the left and right contrasts in the anterior, posterior, and left hemicords. *$p < 0.05$ and **$p < 0.01$. A = anterior, P = posterior, L = left, and R = right.

Table 1

Subject level localization of the activity.

A. Localization of the Activity to the Left or Right Hemicords

Contrast	Number of Subjects with LR Index > 0	Median LR Index	IQR	z-score	p-value
Left	7	0.40	0.69	1.023	0.306
Right	**1**	**−0.49**	**0.32**	**−2.756**	**0.006**
Left > Right	**11**	**0.84**	**0.19**	**2.934**	**0.003**
Right > Left	**1**	**−0.88**	**0.33**	**−2.845**	**0.004**

B. Localization of the Activity to the Anterior or Posterior Hemicords

Contrast	Number of Subjects with AP Index > 0	Median AP Index	IQR	z-score	p-value
Left	7	0.19	0.45	0.622	0.534
Right	5	−0.03	0.34	−0.089	0.929
Left > Right	5	−0.14	0.65	0.000	1.000
Right > Left	4	−0.14	0.35	−1.956	0.050

C. Localization of the Activity to the Ipsilateral Hemicord

Analysis	Number of Subjects with Laterality Index > 0	Median Laterality Index	IQR	z-score	p-value
Task	**11**	**0.84**	**0.16**	**2.934**	**0.003**
Task Control	7	0.15	0.29	0.663	0.508
Task Free Control	5	0.00	0.34	0.153	0.878

A) Left-right (LR) indices were calculated for each of the contrasts. For the LR index, a value of +1.0 indicates that all active voxels were located in the left hemicord while a value of −1.0 indicates that all active voxels were located in the right hemicord. No significant localization of the activity to the left or right hemicord was present for the left contrast; however, for the right contrast, the activity was significantly localized to the right hemicord. For both the left > right and right > left contrasts, the activity was significantly localized to the hemicord ipsilateral to the task. B) Anterior-posterior (AP) indices were calculated for each of the contrasts. For the AP index, a value of +1.0 indicates that all active voxels were located in the anterior hemicord while a value of −1.0 indicates that all active voxels were located in the posterior hemicord. No significant localization of the activity to the anterior or posterior hemicords was present for any of the contrasts. C) For the task, task control, and task free control, laterality indices were calculated for the combined left > right and right > left contrasts. For the laterality index, a value of +1.0 indicates that all active voxels were located in the hemicord ipsilateral to the task while a value of −1.0 indicates that all active voxels were located in the hemicord contralateral to the task. The task demonstrated significant lateralization of the activity to the hemicord ipsilateral to the task while no lateralization of the activity was present for the task control or task free control.

IQR = interquartile range.

Bold font represents $p < 0.05$.